

Chandra Observations of the Pleiades Open Cluster: X-ray Emission from Some Late-B to Early-F stars

Kathryne J. Daniel^{1,2}, Jeffrey L. Linsky², and Marc Gagné¹

kdaniel@wcupa.edu, jlinsky@jila.colorado.edu, mgagne@wcupa.edu

ABSTRACT

We present the analysis of a 38.4 ks and a 23.6 ks observation of the core of the Pleiades open cluster. The Advanced CCD Imaging Spectrometer (ACIS-I) on board the *Chandra* X-ray Observatory has revealed 99 X-ray sources in a $17' \times 17'$ region, including eighteen (of 23) Pleiades members. Fifty-seven sources have no optical or near-infrared counterparts to limiting magnitudes $V= 22.5$ and $K= 13.5$. The unidentified *Chandra* sources are probably background AGN and not stars. The *Chandra* field of view contains seven intermediate mass (B6–F4) cluster members. Four of the intermediate mass members, HII 980 (B6 IV), HII 956 (A7 V), HII 1338 (F3 V), and HII 1122 (F4 V), are X-ray luminous, have soft X-ray spectra, and show no obvious signs of flaring. K- and M-type cluster members with comparable X-ray luminosities have harder X-ray spectra and exhibit moderate flares. For non-flaring K- and M-type stars, L_X is 1–2 orders of magnitude lower than the B- and A-type stars. HII 1284 (A9 V), has X-ray properties comparable to non-flaring K-type stars, and HII 1362 (A7 V) and HII 1375 (A0 V) are not detected. Despite the low number statistics, some late-B to early-F stars in our Pleiades sample (HII 980, HII 956, HII 1122, and HII 1338) appear to be intrinsic X-ray sources. Some late-B to early-F stars, like HII 1284, may have late-type companions, and some, like HII 1362 and HII 1375, may be single, non-X-ray emitting stars. X-ray spectra and light curves of a larger sample of stars are needed to confirm this trend. The X-ray properties of five candidate Pleiades members confirm their cluster membership.

Subject headings: X-rays: stars — open clusters and associations: individual (Pleiades) — stars: activity — stars: early-type — stars: coronae

¹Department of Geology and Astronomy, West Chester University, West Chester, PA 19383

²JILA, University of Colorado and NIST, Boulder, CO 80309-0440

1. Introduction

Magnetic dynamo theories predict that an interaction between differential rotation and sub-photospheric convection creates large photospheric magnetic fields (Parker 1955). These magnetic fields interact in stellar coronae to produce X-ray emission and flares (Pallavicini et al. 1981). Because an outer convective envelope is essential for producing dynamo driven magnetic activity, stars with radiative outer envelopes (hotter than \sim A2) (Bohn 1984) and stars with thin outer convective envelopes (late-A to early-F) do not show a strong correlation between X-ray emission and rotation as would be expected for coronal magnetic activity (Walter 1983). Various theories, such as chromospheric heating through the dissipation of acoustic and MHD waves (Stein 1981; Narain & Ulmschneider 1990), have been suggested to explain X-ray activity from late-A to early-F type stars (see discussion in §4.2).

One of the early surprises from the *Einstein* mission was the detection of strong X-ray emission from O stars, with X-ray luminosity highly correlated with bolometric luminosity (Harnden et al. 1979). Lucy & White (1980) suggested that shock heated clumps could form in the radiatively driven winds of OB stars, possibly leading to X-ray emission. More recent instability-driven wind shock models (Owocki, Castor & Rybicki 1988; MacFarlane & Cassinelli 1989; Hillier et al. 1993; Feldmeier et al. 1995; Cohen et al. 1996; Owocki & Cohen 1999) have been able to explain the X-ray properties of many O and early-B stars with sufficiently high mass-loss rates.

The two leading explanations for X-ray emission, instability-driven wind shocks and dynamo driven magnetic activity, probably cannot produce strong X-rays for stars in the approximate spectral range B3–early-F (Stauffer et al. 1994). Nonetheless, moderate X-ray emission from late-B to early-F stars has been reported for nearly twenty years (e.g., Caillault, Gagné & Stauffer 1994; Huélamo et al. 2001, and references therein). For example, in *Einstein* (Caillault & Helfand 1985; Micela et al. 1990), *ROSAT* (Stauffer et al. 1994; Gagné, Caillault & Stauffer 1995; Micela et al. 1996, 1999), and *Chandra* (Krishnamurthi et al. 2001) studies of the Pleiades, some fraction (10–50%) of late-B to early-F stars were detected. Two explanations have been suggested: the X-rays are produced in the coronae of unseen late-type companions (as first suggested by Golub et al. 1983) or these stars are intrinsic X-ray emitters. The late-type companion hypothesis is difficult to disprove because close binaries are not resolved in X-ray images and spectroscopic binaries are not resolved with high-resolution X-ray grating spectra.

Several studies of the X-ray emission from B- and F-type stars have examined the late-type companion hypothesis in detail. In a *ROSAT* study of A-type stars, Panzera et al. (1999) could not identify conclusively the source of the X-ray emission. Micela et al. (1999) concluded that all the B-type stars detected in the Pleiades are known or possible binaries,

thereby supporting the late-type companion hypothesis. Similarly, in an *Einstein* survey of the Pleiades, Caillault & Helfand (1985) concluded that the X-ray emission from the \sim A6 star, HII 1384, could be attributed to a late-type companion. Simon, Drake & Kim (1995) used archival *ROSAT* data to study ten A-type stars, of which five are associated with known late-type companions. In this study, Simon et al. (1995) concluded that the remaining five must have late-type companions. Stauffer et al. (1994) performed a *ROSAT* survey of the Pleiades showing inconclusive results on this subject. Finally, in *Einstein* and *ROSAT* studies of B6-A3 stars in the Orion Nebula, Caillault & Zoonematkermani (1989) and Stauffer et al. (1994) proposed that the X-ray emission from these stars could be attributed to T-Tauri stars. As Caillault & Zoonematkermani (1989) also suggested, the current models for X-ray emission may need to be revised, as none of these studies could prove or disprove the late-type companion hypothesis.

Several studies have suggested that late-B to early-F stars are intrinsic X-ray emitters. In studies by Micela et al. (1996), Stauffer et al. (1994), and Caillault & Helfand (1985), the A star, HII 1384 (see above), exhibits steady, intense X-ray emission. There is no known companion to this star, as noted by Micela et al. (1990, 1996). An analysis by Berghöfer & Schmitt (1994), using data from the *ROSAT* all-sky survey of B stars with known late- or early-type companions, showed that most of the X-ray flux from these systems was emitted by the early-type stars and not late-type companions. A similar examination of visual binaries was performed by Schmitt et al. (1993) using *ROSAT* HRI pointing data. Here again, the dominant X-ray emission was from late B-type stars. Schmitt (1997) analyzed observations of A- through G-type stars from the *ROSAT* all-sky survey. He consistently found X-ray emission from stars later than \sim A7 and concluded that shallow convection zones were sufficient to produce X-ray emission.

The Pleiades is the prototypical young open cluster. It contains a co-eval (\sim 100 Myr old) population of early- and late-type stars at approximately the same distance (\sim 127 pc, Stello & Nissen 2001; Stauffer et al. 1994) with constant reddening ($E(B - V) \approx 0.03$) in all but the northwest corner of the cluster (Stauffer et al. 1994). Pleiades membership probabilities have been determined in a number of studies using lithium abundances and proper motion. In this paper, we use a pair of deep *Chandra* ACIS-I observations centered on the core of the Pleiades cluster to further examine the X-ray characteristics of early- and late-type cluster members.

2. Data Acquisition and Reduction

Chandra observed the core of the Pleiades open cluster for a total of 56.4 ks. The data

consist of a 34.8 ks exposure using the Advanced CCD Imaging Spectrometer (ACIS) detector acquired on 1999 September 18 (Krishnamurthi et al. 2001) and a 21.2 ks exposure obtained on 2000 March 20. *Chandra*’s high-resolution mirror assembly and ACIS are described in “The Chandra Proposers’ Observatory Guide.” The ACIS-I CCDs (I0-I3) and two CCDs on the ACIS-S array (S2-S3) continuously collected 3.24 s exposures with \sim 40 ms read-out intervals. The I3 aim-points were at (J2000) $\alpha = 3^{\text{h}}46^{\text{m}}45\text{s}.6$, $\delta = +24^{\circ}04'31''$ and $\alpha = 3^{\text{h}}46^{\text{m}}48\text{s}.7$, $\delta = +24^{\circ}04'57''$ for the 1999 and 2000 observations, respectively.

2.1. Data Reduction

We reduced the data using methods available through version 1.1.3 of *Chandra Interactive Analysis of Observations* (CIAO) software, beginning with the second level event list.³ Events with standard *ASCA* grades (0, 2, 3, 4, and 6) were retained. Several hot columns were visible in each observation that had not been removed during the original reduction process. We extracted 14 “hot columns” per observation and six additional columns per CCD near node boundaries. Subtracting these columns from the original 6144 columns resulted in a $\sim 0.8\%$ data loss. We used the aspect histograms and the incident spectrum of a typical Pleiades X-ray source to generate energy-corrected exposure maps. From these we produced a map of the effective exposure time over both observations. We used this final exposure map to calculate the count rate for each source.

ACIS event lists often contain “flaring pixels”: 2-7 localized high-energy events in consecutive read-out frames. Using Takamitsu Miyaji’s C-program, *flagflare*,⁴ all events with flare values < 1 were removed. Tsuboi & Gaffney (2000) show that $\sim 5\%$ of the counts from real events may be removed by using *flagflare*.

Finally, the front-side illuminated CCDs were damaged by radiation early in the mission. The consequent charge transfer inefficiency (CTI) affects the gain and energy resolution (Townsley et al. 2000) of ACIS. We corrected the event lists for each observation using software provided by the *Chandra* X-ray Center.

³An “event list” is a file cataloging each photon’s position at impact with *Chandra*’s CCD camera, time of arrival and the energy. The *Chandra* X-ray Center performs preliminary reduction processes on the data resulting in a “second level” event list.

⁴*flagflare* is available at <http://www.astro.psu.edu/xray/acis/recipes/clean.html>.

2.2. Source Extraction

For each dataset we generated three 1400×1400 pixel images: with $0.5''$, $1''$ and $2''$ pixels. The ACIS-S CCDs were far off-axis for these observations. As a result of vignetting and the large point-spread function (PSF), no new sources were detected; the ACIS-S data are not presented in this paper. The first and second epoch images were registered with respect to the 1999 September images. The resulting co-added images were sharp and showed no signs of systematic astrometric errors. Figure 1 shows a $1400'' \times 1400''$ image with $1''$ pixels of the Pleiades with a logarithmic stretch.

Using these co-added images and exposure maps, we detected 99 *Chandra* sources by applying CIAO’s wavelet-based algorithm tool, *wavdetect*. *Wavdetect* was applied to each image at scales 2, 4, and 8, where the scaling factors are defined as wavelet radii in pixels. Using a false alarm probability of 10^{-6} , we should detect < 2 spurious sources per image. We acquired the greatest coordinate accuracy for each source detection by using scaling factors in accordance with the PSF, and therefore off-axis angle.

The individual source lists from 1999 September and 2000 March were visually compared to the co-added source list. We found that twenty-three new sources appeared as a result of the co-added image’s increased S/N. An additional twenty-two *wavdetect* detections were clearly artifacts of the detection algorithm: these detections were lined up along the edge of the FOV, having been detected because the counts inside the source region were significantly higher than the background outside the FOV. None of these twenty-two positions corresponded to known optical stars. In three cases, a 3–4 count source with no optical candidate was detected in one of the two individual exposures, but not in the co-added image. These three were eliminated because no other other 3–4 count sources were detected. We removed a five count detection because it was over $5'$ off-axis (where the PSF is larger) and no sources with fewer than seven counts had optical counterparts. Table 1 lists the IAU-approved name, position, X-ray counts, associated 1σ statistical uncertainty in the measured counts, and corrected count rate (counts s^{-1}) for the 99 *Chandra* sources in the $17' \times 17'$ FOV.

The resulting 90%-power ellipses were used to extract 99 individual event lists from which we extracted the hardness ratio, Kolmogorov-Smirnov time-variability statistic, light curves and spectrum for each source. We could only use second-epoch data for HHJ 257 (CXOP J034655.6+235622) and first-epoch data for SCG94 171 (CXOP J034716.9+241233), because of slight differences in pointing position. Additionally, it should be noted that HII 956 (CXOP J034615.8+241122) dithered on and off the CCD during the second-epoch observation.

3. Data Analysis

3.1. Source Matching

We constructed a database of all known optical (Martín et al. 2000; Stauffer et al. 1998; Hambly, Hawkins & Jameson 1993; Haro, Chavira & Gonzalez 1982; Hertzsprung 1947; USNO-A 2001), infrared (Martín et al. 2001, 2000; Pinfield et al. 2000; Stauffer et al. 1998; Hambly et al. 1993; 2MASS 2001), and X-ray sources (Micela et al. 1999, 1996; Stauffer et al. 1994; Caillault & Helfand 1985) in the ACIS-I FOV. The position uncertainties used to cross-reference previously cataloged sources are listed in Table 2. *Chandra* position uncertainties are defined by the PSFs described above.

The FOV contains 376 objects, 57 of which are unidentified *Chandra* sources. Of the 99 *Chandra* sources, seven are only associated with known infrared sources, thirteen with only optical sources, and 28 with sources detected both in the optical and infrared. There are no brown dwarf candidates in the *Chandra* FOV. Alternate identifications and spectral data (from Micela et al. 1996, 1999; Haro et al. 1982) are listed in Tables 3 and 4. *Chandra* detected all 34 *ROSAT* sources in the ACIS-I FOV, 26 of which exhibit flare-like activity. In Table 3 we cross-reference each *Chandra* source with all corresponding entries from previous catalogs. In six cases, single sources from other X-ray catalogs were resolved into two or three sources with *Chandra*.

3.1.1. Pleiades Members

Chandra detected eighteen of the 23 bona fide Pleiades members and all five of the possible Pleiades members in the ACIS-I FOV (Pinfield et al. 2000; Belikov et al. 1998; Stauffer et al. 1998; Micela et al. 1996; Schilbach et al. 1995; Hambly et al. 1993). In this paper, Pleiades membership is defined by stars with a proper motion probability (ppm) $> 50\%$ consistent with the known proper motion of the Pleiades cluster. Possible members are stars with similar photometric properties as Pleiades members but where ppm $< 50\%$. In Figure 1, the Pleiades members are outlined on the ACIS-I image. X-ray emission can be associated with five (of seven) early-type Pleiades members (B6 IV, A7 V, A9 V, F3 V, F4 V), and thirteen (of sixteen) late-type stars (K-M) during these observations (Micela et al. 1999, 1996; Haro et al. 1982).

A spectral analysis of seven X-ray luminous Pleiades members revealed that there is a systematic, linear dependence of flux on the HR(see §3.2) of a given source. The flux

conversion factor (FCF) can then be expressed as,

$$\text{FCF} = 1.5 \times 10^{-11} \times \text{HR} + 1.03 \times 10^{-11}. \quad (1)$$

Using this FCF, the X-ray luminosities (L_X) were determined for all detected Pleiades members (for 0.5–8.0 keV).

We calculated L_X upper limits for Pleiades members not detected by *Chandra*. Assuming a constant background, we used detection limits corresponding to the faintest source in a given off-axis radial band (d); the faintest sources where $0' \leq d < 5'$ have 7 cts, $5' \leq d < 10'$ have 10 cts, and $d > 10'$ have 24 cts. We then used the respective 95% confidence level (where 2σ corresponds to a 97.72% confidence level) upper limits for sources of $6_{11.84}^{2.61}$, $9_{15.71}^{4.70}$, and $23_{32.59}^{15.72}$ counts given by Gehrels (1986) to compute the L_X upper limits. For these calculations we used a constant HR corresponding to the mean HR of detected Pleiades members (HR = 0.04) and the effective exposure time at that source's location (see §2.1).

All of the undetected Pleiades members (HCG 254, HII 1362, HII 1375, MHO 10, and MHO 11) were located near the edge of the ACIS-I FOV. The distribution of undetected Pleiades members is illustrated by boxes in Figure 1. As mentioned above (§2.2), the point-source sensitivity of ACIS-I decreases as the PSF increases and effective area decreases with distance from the *Chandra* I3 aim-point. These effects may explain the non-detection of these Pleiades members. It should be noted, however, that despite repeated observations (Micela et al. 1999, 1996; Stauffer et al. 1994; Caillault & Helfand 1985), these sources have not been detected with other X-ray observatories. Thus these undetected sources, which must have low X-ray luminosities, might have been detected by *Chandra* if they were near the aim-point. Table 5 shows spectral data and spectral types for all Pleiades members and possible members not detected during these *Chandra* observations.

3.2. Variability, Hardness Ratios and Spectra

The cleaned event files list the arrival time, energy, and position of each X-ray photon. A cumulative count distribution, $f_n(t)$, for each source was used to calculate the Kolmogorov-Smirnov statistic (KS) assuming a constant count rate, $f_o(t)$, (Babu & Feigelson 1996),

$$\text{KS} = \sqrt{n} \max |f_n(t) - f_o(t)|, \quad (2)$$

where n is the number of photon events and t is the time of arrival. We computed the KS statistic for each source during the first and second observations to look for short term variability. We used the CIAO tool *lightcurve* to extract light-curves for each source and

found that short-term and flare-like variability was correlated with $KS \geq 1.00$. In Table 1, KS_s is the larger of the KS values from 1999 September and 2000 March.

The ~ 6 month interval between 1999 September and 2000 March allowed us to search for long-term variability. We concatenated the two event lists by subtracting the ~ 6 month gap from the second set of photon arrival times. The resulting long-baseline statistic, KS_l , is listed in Table 1. We assume significant long-term variability and no significant short-term variability if $KS_l > 1.00$ and $KS_s < 1.00$. There are 17 such sources in our sample. As noted in §2.2, KS_l is not calculable for HII 956, HHJ 257, and SCG94 171 because the sources were only visible during one *Chandra* observation.

We have compared the L_X values inferred for the six K stars and two F stars in our sample that were also observed with the ROSAT PSPC and analyzed by Gagné et al. (1995). Five of the stars have nearly identical X-ray luminosities, but three of the K stars are factors of 2.1–2.5 times fainter than observed by ROSAT. This magnitude and frequency of variations is consistent with the result found by Schmitt et al. (1993) that $\sim 40\%$ of the Pleiades sources are variable by a factor of 2 in an 11 year time span.

The hardness ratio is defined by,

$$HR = (\text{hard} - \text{soft}) / (\text{hard} + \text{soft}), \quad (3)$$

where soft and hard counts are defined as ACIS events with energies between 0.5–1.0 keV and 1.0–8 keV, respectively. Soft sources show $HR < 0.0$ and hard sources show $HR \geq 0.0$. We compute the error (σ_{HR}) assuming 1σ Poisson statistics from the combined event lists. Table 1 tabulates KS_s , KS_l , HR , and σ_{HR} for each source.

Using the variable-abundance APEC model in XSPEC version 11.0 we modeled ACIS spectra of the six most X-ray luminous Pleiades members in our FOV: HII 956 (A7 V), HII 980 (B6 IV), HII 1355 (K6 V), HII 1122 (F4 V), HII 1124 (K3 V) and HII 1094 (K V). The spectral differences between the 1999 and 2000 observations were significant enough that models of the combined data were not quantitatively accurate. Therefore, the best-fit VAPEC parameters for each of the above stars, with 1σ uncertainties, listed in Table 6 correspond to the individual observations. However, for a qualitative analysis, the ACIS spectra and model fits from the combined dataset are plotted in Figures 2a-f.

These spectra were best fit with a column density of $N_H = 3.6 \times 10^{20} \text{ cm}^{-2}$, in agreement with the reddening to the cluster and previous column density estimates (Caillault & Helfand 1985; Stauffer et al. 1994; Krishnamurthi et al. 2001). For three stars (HII 1094, HII 1124, and HII 1355) single-temperature models yielded $\chi^2 > 2.0$. Since the S/N of these spectra were not sufficient to constrain a two-temperature model with 9 free parameters, the Mg abundance was fixed at 1.00, the column density was fixed at $N_H = 3.6 \times 10^{20} \text{ cm}^{-2}$, and the

upper temperature was fixed at $kT = 3.5$ keV. We note that the excess emission near 0.7 keV in the spectrum of HII 956 (Fig. 2d) gave rise to $\chi^2 \approx 1.6$ for both one- and two-temperature models.

4. Results and Discussion

4.1. Background AGN

Background active galactic nuclei (AGN) are generally detected in ACIS images, and the deep imaging capability of *Chandra* above 2–3 keV makes it possible to observe substantial populations of background AGN even through high column densities.

Unfortunately, because the distant sources show few counts (~ 7 –171 photons), we cannot reliably discriminate between AGN and faint background stellar populations from the shape of their spectra. However, measurements of the HR and count rate are powerful tools for identifying background AGN, as they appear as hard sources with low count rates. In Paper I (Krishnamurthi et al. 2001, and references therein), we estimate that ultra-soft AGN would have $HR > -0.32$, while most X-ray active AGN have $HR > \sim 0$. Stellar sources have $HR \geq 0.35$. While HR alone cannot distinguish between stars and AGN, AGN typically have higher HR values. Figure 3 illustrates this population of unidentified, hard sources with low count rates.

In the *Einstein* Medium-Sensitivity Survey (EMSS) (Stocke et al. 1991), AGN show $-1.0 \leq \log(f_x/f_v) \leq 1.2$, whereas nearly all stars in the EMSS are much less active at X-ray wavelengths: $\log(f_x/f_v) \leq -1.0$. To calculate the maximum expected X-ray flux from a star below the optical completeness threshold, we used the current upper limits (Stauffer et al. 1998, $V = 22.5$) and Equation A3 from Maccacaro et al. (1988),

$$\log(f_x/f_v) = \log(f_x) + \frac{V}{2.5} + 5.37. \quad (4)$$

A very X-ray active star at the completeness threshold of Stauffer et al. (1998) would produce approximately three ACIS counts in our 56.4 ks *Chandra* observation. We conclude that most of the unidentified X-ray sources are not coronal stars. Table 4 also shows a population of ten optically faint ($V > 22.5$, $R > 20.2$ or $J > 14.5$) X-ray sources whose $\log(f_x/f_v)$ values also exceed -1. Figure 3 illustrates that both the unidentified X-ray sources and most of the optically faint X-ray sources have similar X-ray properties (low count rates, low KS values, and high HR values). At this flux level and at this galactic latitude, the most likely candidates for both populations are the optically faint, X-ray active AGN.

We also note that the candidate AGN do not show medium- to large-amplitude short-term variability, as seen on the late-type stars, and have low KS values. This is consistent with known AGN activity since AGN generally show only low-amplitude variability on time-scales ≤ 1 day (Zamorani et al. 1984). For faint AGN, this type of low-level variability would not be evident in a light curve and would yield low KS statistics.

A *Chandra* observation of the Hubble Deep Field-North (Hornschemeier et al. 2001) analyzed the X-ray properties of 82 sources associated with the $8.6' \times 8.7'$ area covered by the Caltech Faint Field Galaxy Redshift Survey. We compared our data to those of Hornschemeier et al. (2001) by assuming $FCF_{AGN} = 1.33 \times 10^{-11} \text{ ergs cm}^{-2} \text{ s}^{-1}$ per ct s^{-1} for a typical AGN candidate. We found that the AGN candidates in our observation have full band ($0.5 - 8.0$ keV) fluxes of $4 \times 10^{-14} < f_{AGN} < 2 \times 10^{-15} \text{ ergs cm}^{-2} \text{ s}^{-1}$. These flux levels encompass 26 sources in $\sim \frac{1}{4}$ of the ACIS-I FOV (Hornschemeier et al. 2001). Therefore, in the direction of the Pleiades, we expect to find < 100 AGN in our FOV. The column density through the Galaxy, in the direction of the Pleiades is $N_H \approx 1.1 \times 10^{21} \text{ cm}^{-2}$ (Dickey & Lockman 1990).

Our source detections give a population of fifty-seven AGN candidates that have not been detected at any other wavelength, and ten optically faint AGN candidates; all of these show $HR \geq -0.32$ and $KS_s \leq 1.5$. Five of these have previously been detected with *ROSAT* (Stauffer et al. 1994). Two of the AGN candidates show $HR \geq 0.35$. In Figure 3 it is obvious that stellar sources (namely Pleiades members) populate the same region of the diagram as candidate AGN. The reader should note the relatively large σ_{HR} values associated with these sources. Every source in Table 1 without an optical or infrared identification is an AGN candidate. Additionally, X-ray detected sources with measured optical and/or infrared magnitudes and with $-1.0 \leq \log(f_x/f_v) \leq 1.2$ are marked as AGN in Table 4.

4.2. Are B- and A-type stars intrinsic X-ray sources?

Of the 23 bona fide Pleiades members present in the ACIS-I FOV, *Chandra* detected eighteen including one B6 IV, two A-type, two F-type, seven K-type, and five M-type stars. One detected but optically faint Pleiades member (HHJ 92) had no listed spectral type, but its color indicates that it is a late-type star. No identified Pleiades G stars are present in our FOV. Based on this sample of stars, we examine the question of whether B4-F5 type stars are intrinsic X-ray emitters, or whether the X-ray emission observed from some of these stars comes rather from unseen late-type companions.

Theoretical stellar structure models (Bohn 1984, e.g.,) show that sub-photospheric con-

vective zones decrease in thickness with increasing T_{eff} and disappear entirely for main sequence stars at $T_{\text{eff}} \approx 9000$ K, corresponding to spectral type A2 V. Although the precise temperature where convection disappears depends on gravity, metal abundance, and the mixing length or other convection parameters, all theories show a rapid decrease in convective zone thickness from the F stars to the early-A stars. This is important because the presence of a turbulent convective layer is usually thought necessary to drive a magnetic dynamo. Also, the turbulent motions in a convective zone continually shuffle the foot-points of magnetic flux tubes, leading to field reconnection events (flares and micro-flares) in the corona and thus heating. Convective motions propagate outward in an atmosphere also leading to heating by the dissipation of acoustic and MHD waves. Field reconnection events and wave dissipation are the mechanisms typically assumed to heat the chromosphere and coronae of low mass stars.

However, in 1991, Simon & Landsman (1991) used the IUE to find lower chromospheric C II 1335Å emission in late-A to early-F stars. Soon after, Walter, Matthews & Linsky (1995) found C II 1335Å from α Aql (A7 IV-V) and α Cep (A7 IV-V). The discovery of lower chromospheric N V 1239Å emission from α Aql and α Cep, and chromospheric Si III 1206Å emission from α Aql, α Cep, and τ^3 Eri (A4 V) (Simon & Landsman 1997) confirmed that some stars as early as A4 V have an active upper atmosphere. Additional observations by Rachford (1997, 1998, 2000) confirmed chromospheric He I 5876Å (D3) emission in A5–F5 (III–V) stars in the Hyades, Praesepe, Coma, the Pleiades and Alpha Persei. In sum, there exist some late-A to early-F type stars with confirmed chromospheres. This, coupled with the findings of Walter (1983, §1), implies that either (1) the shallow convective zones of these stars are able heat the upper atmospheres through the dissipation of acoustic and/or MHD waves to a much higher degree than expected, or (2) there exists some heating mechanism that is not completely understood or fully incorporated into current theoretical models.

Extremely massive stars are not expected to show dynamo-driven magnetic activity, but the spectral type at which the magnetic or wave mechanisms for coronal heating disappear is not yet identified with any precision. Strong wind shocks on O- and early B-type stars lead to relatively soft, non-variable X-ray emission in very high-mass stars (Owocki & Cohen 1999; Owocki, Castor & Rybicki 1988; Lucy & White 1980). Therefore, current models do not predict X-ray emission from late-B to A-type stars. However, Paper I, Huélamo et al. (2001), Stauffer et al. (1994), Caillault et al. (1994), Berghöfer & Schmitt (1994), Schmitt et al. (1993), Micela et al. (1990), Pallavicini, Tagliaferri & Stella (1990), Caillault & Zoonematkermani (1989), and Schmitt et al. (1985) have all recorded X-ray emission from a small percentage of the observed B and A stars using the *Einstein*, *ROSAT*, and *Chandra* satellites. Micela et al. (1996), Stauffer et al. (1994), Schmitt et al. (1993), Grillo et al. (1992), Caillault & Helfand (1985), and Golub et al. (1983) have proposed that this X-ray

emission from some early-type stars could be explained as emission from previously unknown late-type companions.

The hypothesis that late-B and A-type X-ray sources have late-type coronal companions is difficult to refute on the basis of X-ray luminosity or detection fraction alone. Stauffer et al. (1994) noted that the B- and A-type star X-ray luminosities are comparable to active G- and K-type stars, and the fraction of X-ray emitting B- and A-type stars does not exceed the fraction of B- and A-type stars expected to have close late-type companions. However, with the increased S/N and wider bandpass of *Chandra*, we can revisit the question of B- and A-type star X-ray emission by comparing the X-ray characteristics of B- and A-type X-ray sources with flaring and non-flaring K-type Pleiades members. Since the Pleiades stars are likely co-eval, late-type companions to early-type stars should have the same X-ray properties as single late-type stars. A comparison of the hardness ratios, KS statistics, light curves, X-ray luminosities, and X-ray spectra of early- and late-type Pleiades stars thus should test the hypothesis. In order to do this, we split the Pleiades sources into three categories with similar X-ray properties: low X-ray luminosity stars, high X-ray luminosity K stars, and high X-ray luminosity late-B to early-F stars. X-ray characteristics for these groups are summarized in Table 7.

4.2.1. Low X-ray Luminosity Stars

The X-ray faint (inactive) Pleiades members in Table 7 are characterized by $\log L_X < 28.2$ and $HR \approx 0.0 \pm 0.2$. HII 1284's (CXOP J034704.0+235942) (A9 V) X-ray properties ($\log L_X = 27.58$ and $HR = -0.20 \pm 0.16$) are consistent with X-ray emission from an inactive late-type companion. HII 1284 has been repeatedly observed (Micela et al. 1999, 1996; Stauffer et al. 1994; Caillault & Helfand 1985) and not detected in X-rays.

4.2.2. Active K-type Stars

All X-ray luminous K-type stars in our sample, except for HII 1124, were observed to flare, as shown by Table 7. These stars also have hardness ratios with values between $-0.28 \leq HR \leq -0.15$. Two-temperature VAPEC models are needed to adequately fit the X-ray spectra of most of the active K-type stars (see Figures 2a-c, Table 6, and §3.2), HII 1094 (K V), HII 1124 (K3 V), and HII 1355 (K6), the exceptions being observations during which there were no large-scale flares. Presumably, these plasma components correspond to cooler coronal emission at $kT \approx 0.3 - 0.6$ keV and hotter $kT \approx 3.5$ keV plasma associated with

high- or low-level flaring. HII 1094, HII 1124, and HII 1355 also revealed sub-solar iron abundance relative to solar (0.25 ± 0.08 – 0.52 ± 0.14 , 0.23 ± 0.07 – 0.19 ± 0.06 , and 0.55 ± 0.15 – 0.16 ± 0.12 respectively) (Anders & Grevesse 1989). Both HII 1094 and HII 1355 show super-solar neon (2.5 ± 0.45 and 2.59 ± 0.32 – 1.83 ± 0.61) and silicon (2.0 ± 0.5 and 3 ± 1) abundances relative to solar (see Table 6). The reader should note that the spectral resolution of ACIS-I is relatively low and, therefore, the derived abundances should be interpreted with caution. However, similar abundance patterns are seen in high-resolution grating spectra of the Pleiades moving-group member AB Doradus (K1 V) and in other active late-type stars (Güdel et al. 2001; Drake et al. 2001).

4.2.3. HII 956 (A7 V)

HII 956 is a non-flaring source, has a high X-ray luminosity ($\log L_X = 29.31$), consistent with previous measurements (Micela et al. 1996, 1990; Stauffer et al. 1994; Caillault & Helfand 1985), and a soft spectrum ($HR = -0.48 \pm 0.03$). As noted earlier, we find a marginally acceptable one-temperature fit with $kT = 0.57$ keV (see Figure 2d and Table 6). This spectrum also requires somewhat enhanced abundances (where $\text{Ne} = 1.5 \pm 0.3$ and $\text{Mg} = 1.5 \pm 0.3$ relative to solar).

The X-ray properties of HII 956 do not correspond to those of any K-type stars in this sample. Unlike HII 956, the X-ray luminous K stars in our FOV are hard and show clear flare-like activity (see Table 7). A comparison of the light-curves, in Figure 4, illustrates the difference between the flare-like activity of active K stars and the light curve of HII 956. Additionally, the spectrum of HII 956 only requires a relatively cool one temperature coronal plasma, unlike the active K-type stars which require a second very hot component. Thus, in agreement with Krishnamurthi et al. (2001), we conclude that HII 956 is an intrinsic X-ray emitter. Schmitt et al. (1985) identified another A7 V star, Altair, as an intrinsic soft X-ray source. This field star, which is likely much older than the Pleiades, has an X-ray luminosity ($\log L_X = 27.14$) a factor of ~ 300 smaller than HII 956.

Although A7 V stars may have shallow convection zones, it is not clear that the resulting magnetic dynamo could sustain a 6 MK corona as suggested by the ACIS spectrum of HII 956. HII 956 has repeatedly been detected in X-rays⁵ (Micela et al. 1996, 1990; Stauffer et al. 1994; Caillault & Helfand 1985) and shows steady X-ray emission ($\log L_X \approx 29.8$). No study to date has uncovered a close visual or spectroscopic binary companion.

⁵Caillault & Helfand (1985) incorrectly list HII 956 as an F-type star.

4.2.4. HII 980=Merope (B6 IV)

HII 980 is the most bolometrically luminous star in the *Chandra* FOV, with $\log L_X = 29.60$. Like the A7 V star HII 956, HII 980's X-ray characteristics are not consistent with those of active K stars. HII 980's X-rays are softer ($HR = -0.34 \pm 0.02$) and do not exhibit the flare-like eruptions of the X-ray active K stars, but rather the undulating variability seen on HII 956 (see Figure 4). The X-ray spectrum of HII 980 (Figure 2e and Table 6) requires one plasma with $kT = 0.53$ keV– $kT = 0.59 \pm 0.02$. HII 980 suggests sub-solar iron (0.63 ± 0.05 – 0.69 ± 0.17), super-solar magnesium (1.5 ± 0.2 – 1.39 ± 0.50) and silicon (1.5 ± 0.2 – 1.69 ± 0.74) abundances during both observations, and super-solar neon (1.5 ± 0.3) during the 1999 September 18 observation. Historically (Micela et al. 1996, 1990; Stauffer et al. 1994; Caillault & Helfand 1985), HII 980 has displayed steady, bright X-ray emission ($\log L_X \approx 29.8$). Since the X-ray emission is not consistent with the Pleiades active K stars, we conclude that HII 980 is an intrinsic X-ray source.

4.2.5. HII 1338 (F3 V) and HII 1122 (F4 V)

HII 1338 (F3 V) and HII 1122 (F4 V) have X-ray luminosities consistent with those reported by Stauffer et al. (1994) and Micela et al. (1999, 1996, 1990). We measure $L_X = 28.67$ for HII 1338 and $L_X = 29.06$ for HII 1122. The F-type stars in our sample have hardness ratios ($HR \approx -0.45$) comparable to those of HII 956 ($HR = -0.48 \pm 0.03$) and HII 980 ($HR = -0.34 \pm 0.02$). The light curves of both HII 1338 and HII 1122 are similar to those of HII 956 and HII 980 as shown in Figure 4. The spectrum of HII 1122 (Figure 2f and Table 6) indicates a temperature of $kT = 0.45$ keV, like HII 956 and HII 980. Note also the super-solar magnesium (2.79 ± 0.74) abundance. HII 980 (B6 IV), HII 956 (A7 V), HII 1338 (F3 V) and HII 1122 (F4 V) have four properties which distinguish them from late-type Pleiades members: they are X-ray luminous, have moderate temperatures, have soft HR values, and show no signs of flare-like variability.

4.2.6. Undetected A stars: HII 1375 (A0 V) and HII 1362 (A7 V)

Chandra did not detect HII 1375 (A0 V) or HII 1362 (A7) with a very low upper limit of $\log L_X < 27.98$ and $\log L_X < 27.87$ respectively. As these stars have been repeatedly observed and not detected in the X-rays (Micela et al. 1999, 1996, 1990; Stauffer et al. 1994; Caillault & Helfand 1985, §3.1.1), we conclude that they are not strong X-ray sources and that they do not have active late-type companions. It is interesting to note that while HII 1362 is one

of the earliest known stars to have a detectable chromosphere (Rachford 2000), it was not detected by *Chandra*.

4.2.7. *Detection fraction of flares*

As reported by Gagné et al. (1995), flares detected by *ROSAT* exhibited peak X-ray luminosities in excess of $L_X = 3 \times 10^{30} \text{ ergs s}^{-1}$. Only ten flares were detected from 171 Pleiades members (Gagné et al. 1995; Stauffer et al. 1994) with *ROSAT* (all associated with late-type stars). As a result of its small PSF, increased effective area, and low ACIS-I background, *Chandra* detected flare-like activity on nine of twenty-three Pleiades members on similar time-scales.

Chandra reveals flare-like activity on five of the seven K-type Pleiades members in the FOV. Also, of the seven early-type Pleiades members in the FOV, *Chandra* detected five; none of which show flare-like variability. If the X-ray activity from HII 980, HII 956, HII 1338, and HII 1122 came from an unseen G- or K-type companion, one would expect similar flaring statistics from both populations. As such, it is significant that in every X-ray observation of the Pleiades to date (Krishnamurthi et al. 2001; Micela et al. 1999, 1996; Gagné et al. 1995; Stauffer et al. 1994; Micela et al. 1990; Caillault & Helfand 1985) HII 980, HII 956, HII 1338, and HII 1122 do not exhibit flare-like activity. Thus, while the hypothesis that X-ray emission associated with late-B to early-F type stars originates from unseen late-type companions may be true in some cases, it appears not to be true for these four stars.

4.3. Possible New Pleiades Members

Chandra detected all five of the possible Pleiades members in the ACIS-I FOV. Membership probability was determined by proper motion and photometric properties in agreement with the Pleiades cluster (Belikov et al. 1998; Stauffer et al. 1998; Micela et al. 1996; Schilbach et al. 1995; Hambly et al. 1993; Soderblom et al. 1993, §3.1). Tentative X-ray luminosities have been determined for the possible Pleiades members using the same parameters (including distance) as for the bona fide Pleiades members. These X-ray characteristics are listed in Table 7.

4.3.1. HHJ 140 (M V)

The light-curve of HHJ 140 (CXOP J034635.4+240134) (M V) displays a high amplitude flare during the second observation, exceeding the count rate of the first observation by a factor of 75. This hard source shows $HR = 0.17 \pm 0.03$ and $\log L_X = 29.48$. This is much harder than typical HR values of the active Pleiades late-type stars. However, the hardness of HHJ 140’s spectrum is due to the flare: during the first observation $HR = -0.59$, and during the second $HR = 0.22$. As the second observation contains the majority of the counts, the overall HR value is heavily weighted by the second observation. Since no other sources in these observations show flares of this magnitude, we cannot directly compare the X-ray properties of this source with Pleiades stars. However, the large flare and X-ray luminosity indicate that HHJ 140 is very active, and thus is consistent with being a Pleiades member.

4.3.2. HHJ 195 and HHJ 257

HHJ 195 (CXOP J034623.3+240151) and HHJ 257 (CXOP J034655.6+235622) are both faint X-ray sources showing $\log L_X = 28.13$ and $\log L_X = 28.32$, respectively, if they are located at the distance of the Pleiades. The HR values ($HR = -0.23 \pm 0.11$ and $HR = -0.23 \pm 0.16$ respectively) are also within the range for X-ray faint late-type Pleiades members. These stars have been speculatively included in two membership catalogs (Stauffer et al. 1994; Hambly et al. 1993), but do not have associated membership probabilities. The X-ray properties indicate that these stars lie within the range observed in the Pleiades cluster and are thus likely Pleiades members.

4.3.3. SRS 62618 and SRS 60765

SRS 62618 (CXOP J034643.5+235941) and SRS 60765 (CXOP J034709.1+240307) are candidate Pleiades members in the Schilbach et al. (1995) and Belikov et al. (1998) catalogs. These sources have low proper motion probability, although their photometric properties are consistent with Pleiades membership (see Table 4 and §3.1.1). SRS 62618 and SRS 60765 are relatively soft sources ($HR = -0.23 \pm 0.07$ and $HR = -0.19 \pm 0.16$), with high X-ray luminosities ($\log L_X = 28.67$ and $\log L_X = 29.03$), and high KS_s values ($KS_s = 1.33$ and $KS_s = 3.50$). These stars have X-ray properties of active late-type Pleiades members, suggesting that SRS 62618 and SRS 60765 are Pleiades members and not field stars.

5. Summary and Conclusions

Based on our analysis of the 1999 September and 2000 March *Chandra* ACIS-I observations of the core of the Pleiades cluster,

1. We identify 99 X-ray sources, of which 57 have not been detected at any other wavelength. Hardness ratios, Kolmogorov-Smirnov statistics, and count rates have been derived for all 99 *Chandra* sources.
2. The 57 sources are faint, hard, and have low KS values and are not listed in optical/IR catalogs. They also show $-1.0 \leq \log(f_x/f_v) \leq 1.2$. Additionally, there are ten faint optical/IR sources with similar $\log(f_x/f_v)$. These 67 sources are probably background AGN.
3. The high X-ray luminosity, moderate plasma temperature, low hardness ratios, and non-flaring light curves of HII 980 (B6 IV), HII 956 (A7 V), HII 1338 (F3 V), and HII 1122 (F4 V) indicate that these are either intrinsic X-ray sources or they have unseen low-mass companions with different coronal properties than low-mass Pleiades stars. One possibility that we cannot dismiss at this time is that the B6 IV star may have an unknown companion like the active A7-F4 Pleiades stars that would be 4–5 visual magnitudes fainter and could be in an orbit with no detectable Doppler shift.
4. HII 1284 (A9 V) has X-ray properties comparable to those of K-type Pleiades members. Its X-ray emission may come from an unseen late-type companion.
5. Five Pleiades members are not detected in the combined Chandra image, putting stringent upper limits on the X-ray luminosity of some early- and late-type cluster members. Two of these are Pleiades A stars (A0 V and A7 V). These may be single, non X-ray emitting stars.
6. HHJ 140, SRS 62618, SRS 60765, HHJ 195, and HHJ 257 are likely Pleiades members.

Despite the small sample of Pleiades members in the *Chandra* FOV, a pattern among late-B to early-F stars does emerge: some early-type stars like HII 980, HII 956, HII 1338, and HII 1122 appear to be intrinsic X-ray emitters. Some, like HII 1284, may have late-type companions, and others, like HII 1362 and HII 1375, may be single, inactive stars.

These conclusions are consistent with the previous studies cited in §1. Previous results (e.g., Caillault et al. 1994; Stauffer et al. 1994; Gagné et al. 1995) were consistent with late-type binary companions because the observed X-ray detection fraction did not exceed the

expected binary fraction. We note, however, that the high detection fraction required that essentially all the coronal companions have higher than average X-ray luminosity.

The second argument for unseen late-type companions was that the X-ray properties of the late-B to early-F stars were indistinguishable from late-type coronal sources. The *Chandra* light curves and hardness ratios of some B6–F4 stars are non-flaring and softer than their K-type counterparts. X-ray spectra and light-curves of a larger sample of stars are needed to confirm this suggestion. If confirmed, then new X-ray emission mechanisms, like magnetically confined wind shocks (Babel & Montmerle 1997), may be required.

This study was made possible by NASA grant H-04630D to NIST and the University of Colorado. We are grateful to Anita Krishnamurthi for providing compiled catalogs of sources in this region, and for her helpful comments on imaging. We thank Chris Reynolds for his helpful comments on AGN. We would also like to thank Takamitsu Miyaji for providing the code to eliminate flaring pixels. MG would like to dedicate the AGN candidate J034620.8+235858 to his active daughter Emma, born 8 October 1999. This research made use of the SIMBAD astronomical database operated by CDS at Strasbourg, France.

REFERENCES

Anders E., & Grevesse N. 1989, *Geochimica et Cosmochimica Acta*, 53, 197

Babel, J. , & Montmerle, T. 1997, *A&A*, 323, 121

Babu, G.J., & Feigelson, E.D. 1996, *Astrostatistics* (London: Chapman & Hall)

Belikov, A.N., Hirte, S., Meusinger, H., Piskunov, A.E., & Schilbach, E. 1998, *A&A*, 332, 575

Berghöfer, T.W., & Schmitt, J.H.M.M. 1994, *ApJ*, 292, 5

Bohn, H.U. 1984, *A&A*, 136, 338

Caillault, J.-P., Gagné, M., & Stauffer, J.R. 1994, *ApJ*, 432, 386

Caillault, J.-P., & Zoonematkermani, S. 1989, *ApJ*, 338, L57

Caillault, J.-P., & Helfand, D.J. 1985, 289, 279

Cohen, D.H., Cooper, R.G., Macfarlane, J.J., Owocki, S.P., Cassinelli, J.P., & Wang, P. 1996, *ApJ*, 460, 506

Dickey, J.M., & Lockman, F.J. 1990, *ARA&A*, 28, 215

Drake, J. J., Brickhouse, N. S., Kashyap, V., Laming, J. M., Huenemoerder, D. P., Smith, R., & Wargelin, B. J. 2001, *ApJ*, 548, L81

Eichhorn, H., Googe, W.D., Lukac, C.F., & Murphy, J.K. 1970, *MNRAS*, 73, 125

Feldmeier, A., Puls, J., Reile, C., Pauldrach, A., Kudritzki, R.P., & Owocki, S.P. 1995, *Ap&SS*, 233, 293

Gagné, M., Caillault, J.-P., & Stauffer, J.R. 1995, *ApJ*, 450, 217

Gehrels, N. 1986, *ApJ*, 303, 336

Golub, J., Harnden, F.R., Maxson, C.W., Vaiana, G.S., Snow, T.P., Rosner, R., & Cash, W., Jr. 1983, *ApJ*, 271, 264

Grillo, F., Sciortino, S., Micela, G., Vaiana, G.S., & Harnden, F.R., Jr. 1992, *ApJS*, 81, 795

Güdel, M. et al. 2001, *A&A*, 365, L336

Hambly, N.C., Hawkins, M.R.S., & Jameson, R.F. 1993, *A&AS*, 100, 607 (HHJ)

Harnden, F.R., Jr., et al. 1979, *ApJ*, 234, L51

Haro, G., Chavira, E., & Gonzalez, G. 1982, *Bol. Obs. Tonantzintla Tacubaya*, 3, 3 (HCG)

Hertzsprung, E. 1947, *Ann. Sternw. Leiden*, 19, Part 1 (HII)

Hillier, D.J., et al. 1993, *A&A*, 276, 117

Hornschemeier, A.E., Brandt, W.N., Garmire, G.P., Schneider, D.P., Barger, A.J., Broos, P.S., Cowie, L.L., Townsley, L.K., Bautz, M.W., Burrows, D.N., Chartas, G., Feigelson, E.D., Griffiths, R.E., Lumb, D., Nousek, J.A., Ramsey, L.W., & Sargent, W.L.W. 2001, *ApJ*, 554, 742

Huélamo, N., Brandner, W., Brown, A.G.A., Neuhäuser, R., & Zinnecker, H. 2001, *A&A*, 373, 657

Krishnamurthi, A., Reynolds, C. S., Linsky, J. L., Martín, E., & Gagné, M. 2001, *AJ*, 121, 337 (Paper I)

Lucy, L.B., & White R.L. 1980, *ApJ*, 241, 300

Maccacaro, T., Gioga, I.M., Wolter, A., Zamorani, G., & Stocke, J.T. 1988, *ApJ*, 326, 680

MacFarlane, J.J., & Cassinelli, J.P. 1989, *ApJ*, 347, 1090

Martín, E.L., et al. 2001, *ApJ*, in press

Martín, E.L., Brandner, W., Bouvier, J., Luhman, K.L., Stauffer, J., Basri, G., Zapatero Osorio, M.R., & Barrado y Navascués 2000, *ApJ*, 543, 299

Micela, G., Sciortino, S., Harnden, F.R., Jr., Kashyap, V., Rosner, R., Prosser, C.F., Damiani, F., Stauffer, J., & Caillault, J.-P. 1999, *A&A*, 341, 751

Micela, G., Sciortino, S., Kashyap, V., Harnden, F.R., Jr., & Rosner, R. 1996, *ApJS*, 102, 75 (MSK)

Micela, G., Sciortino, S., Vaiana, G., Harnden, F.R., Jr., Rosner, R., & Schmitt, J.H.M.M. 1990, *ApJ*, 348, 557

Narain, U., & Ulmschneider, P. 1990, *SSRv*, 54, 377

Owocki, S.P., & Cohen, D.H. 1999, *ApJ*, 520, 833

Owocki, S.P., Castor, J.I., & Rybicki, G.B. 1988, *ApJ*, 335, 914

Pallavicini, R., Golub, L., Rosner, R., Vaiana, G.S., Ayres, T., & Linsky, J. L. 1981, *ApJ*, 282, 403

Pallavicini, R., Tagliaferri, G., & Stella, L. 1990, *A&A*, 282, 403

Panzera, M.R., Tagliaferri, G., Pasinetti, L., & Antonello, E. 1999, *A&A*, 348, 161

Parker, E.N. 1955, *ApJ*, 122, 293

Pinfield, D.J., Hodgkin, S.T., Jameson, R.F., Cossburn, M.R., Hambly, N.C., & Dervereux, N. 2000, *MNRAS*, 313, 347 (BPL)

Rachford, B.L. 2000, *MNRAS*, 315, 24

Rachford, B.L. 1998, *ApJ*, 505, 255

Rachford, B.L. 1997, *ApJ*, 486, 994

Schilbach, E., Robichon, N., Souchay, J., & Guibert, J. 1995, *A&A*, 299, 696 (SRS)

Schmitt, J.H.M.M. 1997, *A&A*, 318, 215

Schmitt, J.H.M.M., Zinnecker, H., Crudace, R., & Harnden, F.R., Jr. 1993, *ApJ*, 402, L13

Schmitt, J.H.M.M., Golub, L., Harnden, F.R., Jr., Maxson, C.W., Rosner, R., & Vaiana, G.S. 1985, *ApJ*, 290, 307

Simon, T., & Landsman, W.B. 1997, *ApJ*, 483, 435

Simon, T., Drake, S.A., & Kim, P.D. 1995, *Astronomical Society of the Pacific*, 107, 1034

Simon, T., & Landsman, W.B. 1991, *ApJ*, 380, 200

Soderblom, D.R., Stauffer, J.R., Hudon, J.D., & Jones, B.F. 1993, *ApJ*, 85, 315

Stauffer, J.R., Schild, R., Barrado y Navascués, D., Backman, D.E., Angelova, A.M., Kirkpatrick, J.D., Hambly, N., & Vanzi, L. 1998, *ApJ*, 504, 805 (MHO)

Stauffer, J.R., Caillault, J.-P., Gagné, M., Prosser, C.F., & Hartmann, L.W. 1994, *ApJS*, 91, 625 (SCG94)

Stein, R.F. 1981, *ApJ*, 246, 966

Stello, D., & Nissen, P.E. 2001, *A&A*, 374, 105

Stocke, J.T., Morris, S.L., Gioia, I.M., Maccacaro, T., Schild, R., Wolter, A., Fleming, T.A., & Henry, J.P. 1991, *ApJS*, 76, 813

Townsley, L.K., Broos, P.S., Garmire, G.P., & Nousek, J.A. 2000, *ApJ*, 534, L139

Tsuboi, Y., & Gaffney, J. 2000, Report on Flaring Pixels in ACIS

Walter, F.M., Matthews, L.D., & Linsky, J.L. 1995, *ApJ*, 447, 353

Walter, F.M. 1983, *ApJ*, 274, 794

Zamorani, G., Giommi, P., Maccacaro, T., Tananbaum, H. 1984, *ApJ*, 278, 28

Two Micron All-Sky Survey 2001, 2nd Incremental Release, Point Source Catalog (2MASS)

United States Naval Observatory Catalog A 2001 (USNO-A)

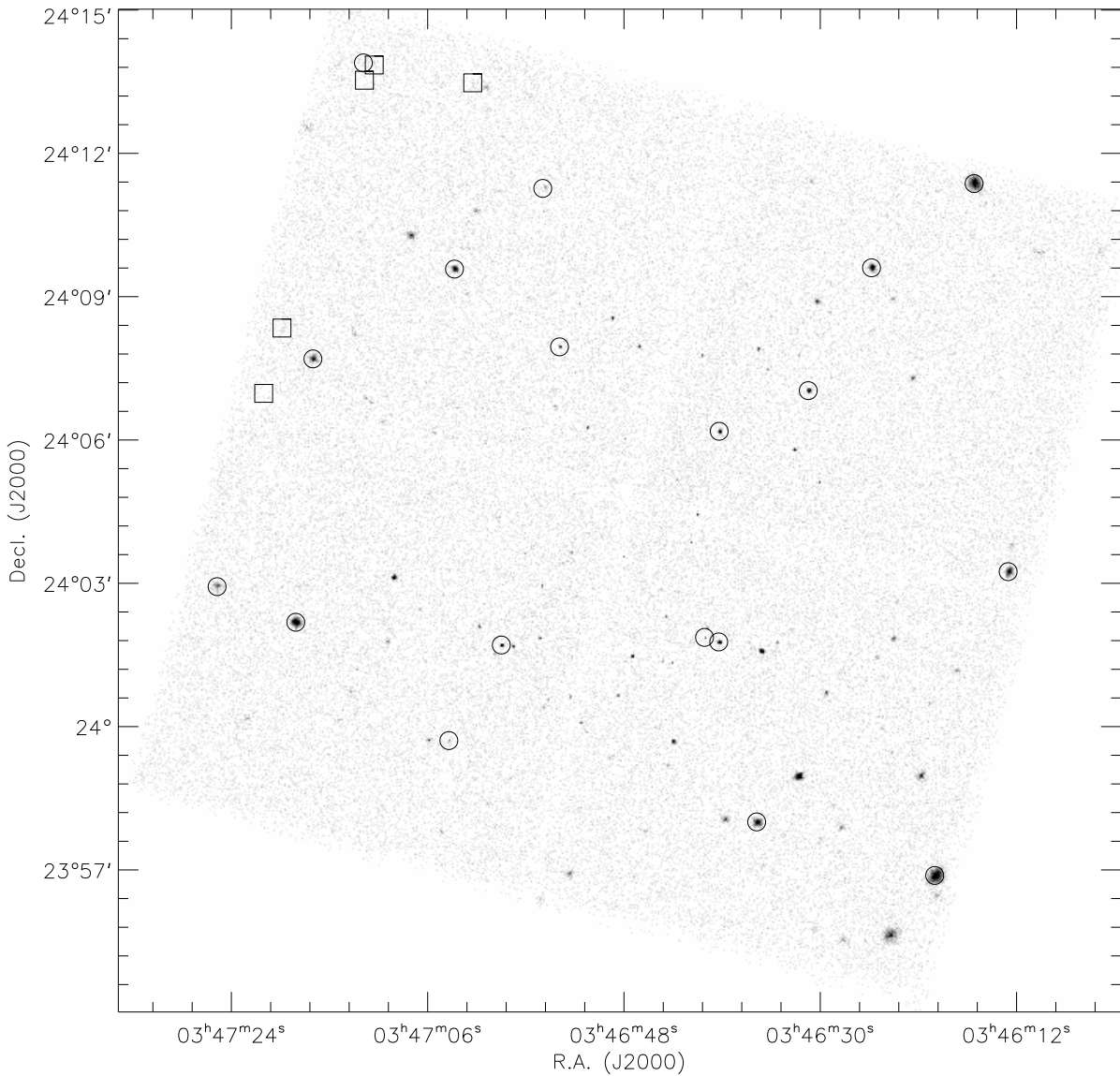


Fig. 1.— This co-added 56.4 ks image of the Pleiades core was taken with ACIS-I on board *Chandra*. Detected Pleiades members are enclosed by circles and undetected Pleiades members are enclosed by squares.

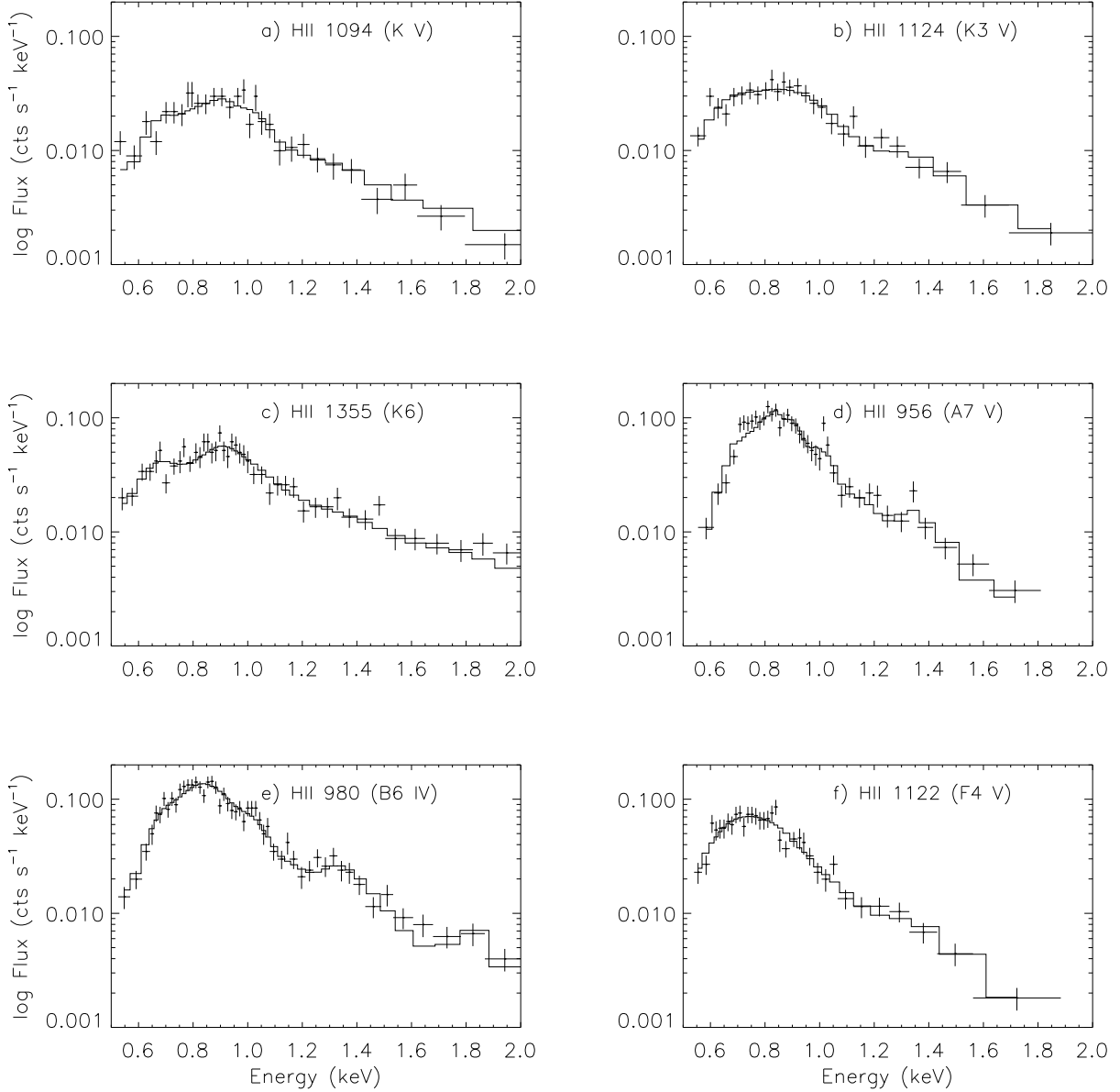


Fig. 2.— Spectra of the six most X-ray luminous Pleiades members in the ACIS-I FOV, assuming a column density of $N_H = 3.6 \times 10^{20} \text{ cm}^{-2}$ to the Pleiades. HII 980, HII 956, and HII 1122 required a single temperature coronal model, while the K-type stars required two temperature models.

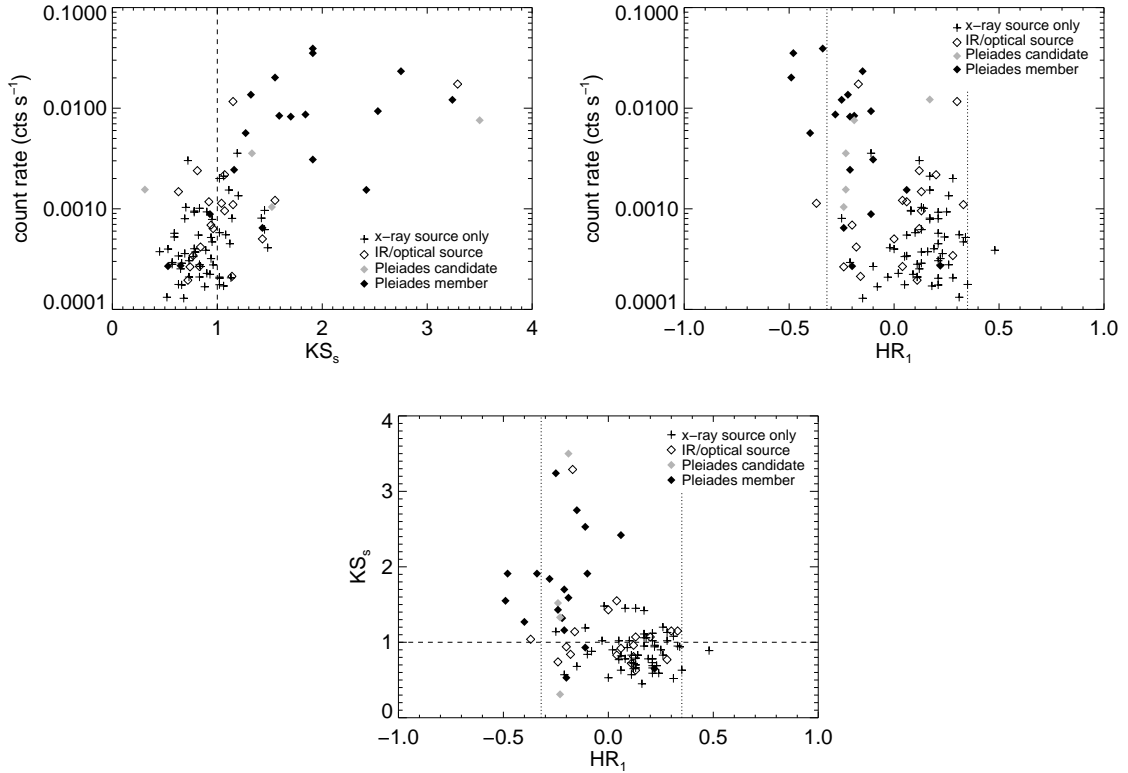


Fig. 3.— These plots of the KS statistic, count rates, and HR values are useful tools in detecting AGN. Ultra-soft AGN could have HR values as small as -0.32 , most X-ray active AGN will show HR values greater than ~ 0 , and sources where $HR \geq 0.35$ are almost certainly AGN. Dotted lines indicate these critical values. The dashed lines mark the threshold between variable and non-variable sources.

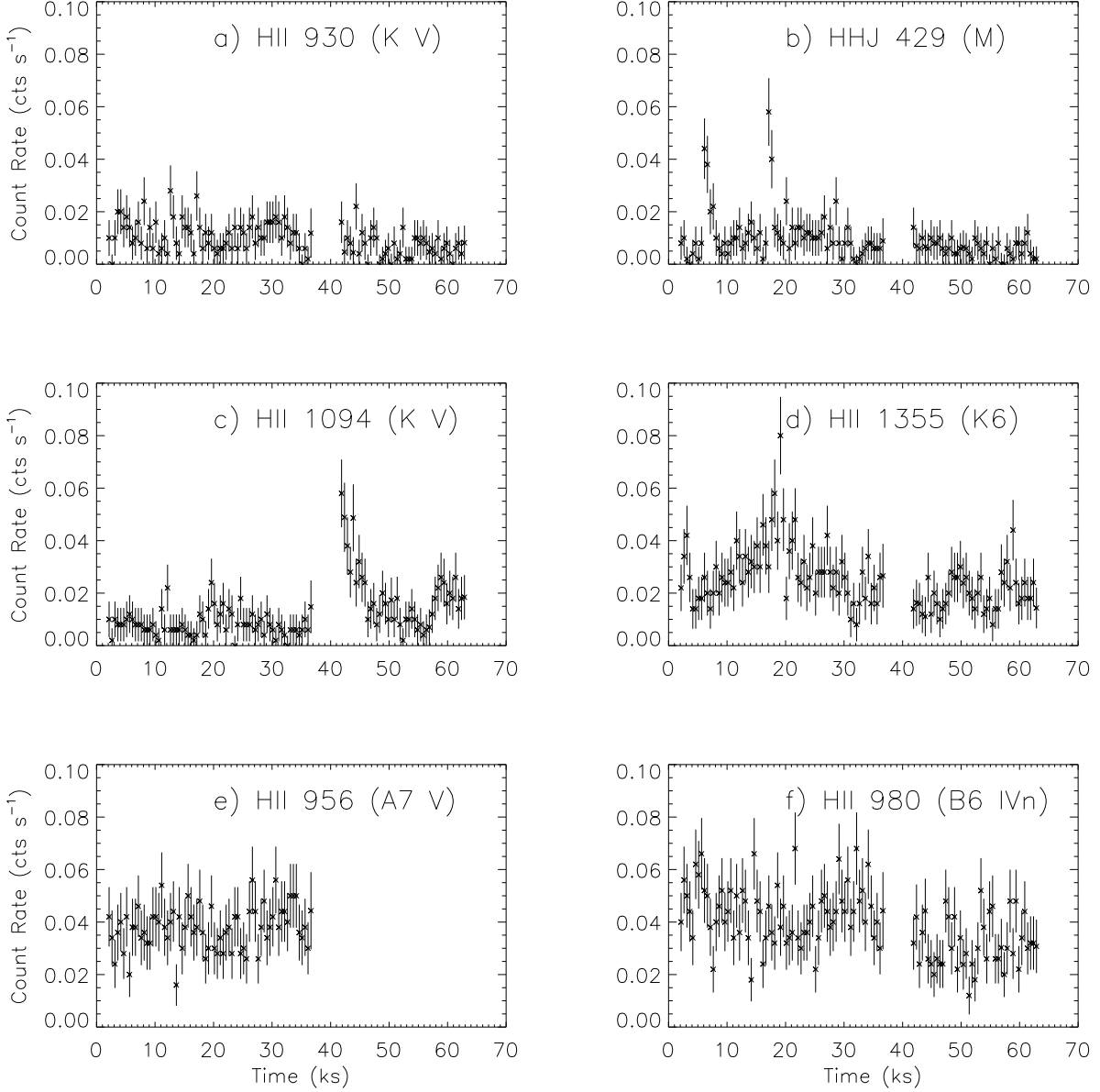


Fig. 4.— ACIS X-ray light-curves of active K-type stars and early-type stars (500 s bins). The data gap represents the six month interval between observations. All of the highly X-ray luminous K stars show flare-like activity. Light-curves (e) and (f) show undulating, short-term variability over the course of a single observation, and larger variability from 1999 September 18 to 2000 March 20. HII 956 (e), HII 980 (f), HII 1122 (not shown), and HII 1338 (not shown) have not exhibited short-term flare-like variability in any of the numerous observations with *Einstein*, *ROSAT*, and now *Chandra*.

Table 1. *Chandra* X-ray sources in the core of the Pleiades.

CXOP	R.A. (J2000)	Decl. (J2000)	counts	error	count rate (cts s ⁻¹)	KS _s	KS _l	HR	σ_{HR}	Name ^a
J034604.5+240957	3 46 04.59	24 09 57.9	32	10	0.000689	0.94	0.49	-0.20	0.10	BPL 88
J034609.9+240541	3 46 09.92	24 05 41.7	11	8	0.000228	0.90	1.79	0.02	0.10	...
J034610.0+240954	3 46 10.01	24 09 54.6	45	9	0.000948	0.78	0.63	0.08	0.07	...
J034612.5+240347	3 46 12.60	24 03 47.3	22	6	0.000450	1.12	1.59	0.21	0.10	...
J034612.7+240314	3 46 12.77	24 03 14.6	411	22	0.008411	1.59	3.71	-0.19	0.04	HII 930
J034615.8+241122	3 46 15.90	24 11 22.0	1344	39	0.035244	1.91	...	-0.48	0.03	HII 956
J034617.6+240110	3 46 17.61	24 01 10.2	38	8	0.000784	0.95	0.79	0.17	0.10	...
J034619.4+235628	3 46 19.45	23 56 28.9	24	8	0.000621	1.45	1.05	0.13	0.10	...
J034619.5+235653	3 46 19.51	23 56 53.0	1825	46	0.039150	1.91	4.73	-0.34	0.02	HII 980
J034620.1+240028	3 46 20.10	24 00 28.8	13	5	0.000267	0.84	0.59	-0.10	0.13	...
J034620.8+235858	3 46 20.85	23 58 58.5	171	16	0.003567	1.19	2.12	-0.11	0.06	...
J034621.5+240717	3 46 21.58	24 07 17.3	68	10	0.001348	1.20	0.96	0.26	0.10	...
J034623.3+240151	3 46 23.37	24 01 51.1	52	9	0.001042	1.52	1.36	-0.24	0.11	HHJ 195
J034623.4+240856	3 46 23.42	24 08 56.9	27	6	0.000552	1.08	0.77	0.31	0.13	...
J034623.6+235538	3 46 23.64	23 55 38.9	542	26	0.011645	1.15	1.35	0.30	0.04	0346237+235540
J034624.3+235958	3 46 24.38	23 59 58.5	13	5	0.000277	0.96	1.43	0.22	0.19	...
J034624.8+240126	3 46 24.88	24 01 27.0	16	6	0.000320	0.94	1.45	0.22	0.17	...
J034625.2+240936	3 46 25.30	24 09 36.2	448	23	0.009348	2.53	4.51	-0.11	0.04	HHJ 429
J034627.9+235532	3 46 27.95	23 55 32.1	57	10	0.001213	1.55	0.92	0.04	0.08	0346379+235525
J034628.1+235753	3 46 28.13	23 57 53.7	50	9	0.001033	0.70	1.47	0.13	0.09	...
J034628.8+235820	3 46 28.89	23 58 20.8	13	5	0.000267	0.83	0.67	0.04	0.13	0346290+235822
J034629.1+240839	3 46 29.18	24 08 39.9	10	4	0.000195	0.72	0.54	0.11	0.24	0346290+240839
J034629.5+240042	3 46 29.53	24 00 42.8	51	8	0.001012	0.83	0.54	0.14	0.11	...
J034630.0+235740	3 46 30.01	23 57 40.1	10	4	0.000206	1.13	1.08	0.28	0.12	...
J034630.1+240507	3 46 30.16	24 05 07.1	22	5	0.000417	0.84	0.95	-0.18	0.17	SRS 64413
J034630.3+240853	3 46 30.35	24 08 53.7	77	11	0.001536	1.11	3.27	0.17	0.09	...
J034630.5+235546	3 46 30.59	23 55 46.9	26	7	0.000548	0.82	1.41	0.06	0.10	...
J034630.8+241124	3 46 30.85	24 11 24.1	17	5	0.000340	0.63	1.28	0.06	0.11	...
J034631.1+240701	3 46 31.10	24 07 02.0	432	23	0.008242	1.70	2.02	-0.21	0.04	HII 1061
J034632.0+235858	3 46 32.04	23 58 58.1	861	34	0.017366	3.29	5.16	-0.17	0.03	HII 1069
J034632.0+240746	3 46 32.01	24 07 46.5	9	4	0.000176	1.02	1.04	0.05	0.21	...
J034632.4+240547	3 46 32.42	24 05 47.7	112	12	0.002108	1.06	0.64	0.17	0.09	...
J034634.0+240146	3 46 34.01	24 01 46.0	20	5	0.000387	0.89	0.66	0.48	0.19	...
J034634.8+240728	3 46 34.88	24 07 28.8	13	4	0.000253	0.65	0.77	0.12	0.20	...
J034635.4+240134	3 46 35.43	24 01 35.0	632	29	0.012193	13.65	19.69	0.17	0.03	HHJ 140
J034635.7+240754	3 46 35.73	24 07 54.5	42	8	0.000798	0.69	0.42	0.21	0.13	...

Table 1—Continued

CXOP	R.A. (J2000)	Decl. (J2000)	counts	error	count rate (cts s ⁻¹)	KS _s	KS _l	HR	σ_{HR}	Name ^a
J034635.8+235800	3 46 35.83	23 58 00.3	571	26	0.012113	3.24	5.68	-0.25	0.04	HII 1094
J034638.7+235804	3 46 38.78	23 58 04.2	119	12	0.002394	0.81	1.33	0.12	0.08	0346388+235805
J034639.2+240610	3 46 39.27	24 06 10.9	1093	34	0.020173	1.55	3.81	-0.49	0.03	HII 1122
J034639.3+240146	3 46 39.31	24 01 46.4	714	29	0.013615	1.32	0.97	-0.22	0.04	HII 1124
J034640.6+240152	3 46 40.62	24 01 52.0	14	4	0.000272	0.65	0.49	0.22	0.24	SRS 64425
J034640.8+240746	3 46 40.89	24 07 46.1	25	6	0.000469	0.95	1.47	0.33	0.16	...
J034641.3+240426	3 46 41.33	24 04 26.4	67	9	0.002001	1.02	2.55	0.28	0.12	...
J034641.8+240351	3 46 41.88	24 03 51.8	20	5	0.000372	0.79	0.82	0.13	0.21	...
J034643.5+235941	3 46 43.52	23 59 41.6	175	14	0.003561	1.33	1.12	-0.23	0.07	SRS 62618
J034643.6+240120	3 46 43.65	24 01 20.5	18	5	0.000343	0.77	0.90	0.28	0.20	U1125_01262845
J034644.0+235911	3 46 44.05	23 59 11.5	14	5	0.000288	0.66	1.43	0.13	0.18	...
J034644.1+240218	3 46 44.19	24 02 18.6	20	5	0.000375	0.45	0.65	0.16	0.20	...
J034644.5+240122	3 46 44.50	24 01 22.2	9	4	0.000171	1.06	0.82	0.18	0.24	...
J034646.0+235750	3 46 46.02	23 57 50.3	16	5	0.000335	0.77	0.47	0.05	0.15	...
J034646.6+240757	3 46 46.65	24 07 57.6	50	8	0.000955	1.07	1.49	0.13	0.12	KECK
J034647.2+240128	3 46 47.27	24 01 28.7	115	12	0.002181	1.07	2.00	0.20	0.09	KECK
J034647.9+240601	3 46 48.00	24 06 01.9	9	4	0.000168	0.88	0.90	-0.08	0.29	...
J034648.1+240334	3 46 48.11	24 03 34.1	13	4	0.000305	0.73	0.85	0.21	0.27	...
J034648.5+240039	3 46 48.59	24 00 39.5	27	6	0.000519	0.94	1.14	0.34	0.17	...
J034649.1+240833	3 46 49.11	24 08 33.0	61	9	0.001175	0.92	0.60	0.06	0.11	KECK
J034651.3+240615	3 46 51.38	24 06 15.8	43	7	0.000803	1.14	1.03	-0.25	0.14	...
J034651.4+235953	3 46 51.49	23 59 54.0	9	4	0.000175	0.66	0.95	0.21	0.19	...
J034652.0+240005	3 46 52.00	24 00 05.2	29	6	0.000636	0.96	1.56	0.12	0.14	KECK
J034652.1+240850	3 46 52.14	24 08 50.7	9	4	0.000177	0.63	0.52	0.35	0.22	...
J034652.8+240338	3 46 52.88	24 03 38.9	16	5	0.000293	0.57	0.45	-0.21	0.20	...
J034652.9+240037	3 46 52.99	24 00 37.6	17	5	0.000571	0.59	1.63	0.21	0.19	...
J034653.0+235656	3 46 53.03	23 56 56.4	73	10	0.001480	0.63	0.65	0.13	0.08	KECK
J034653.6+240325	3 46 53.63	24 03 25.2	7	3	0.000129	0.68	0.96	-0.15	0.28	...
J034653.9+240757	3 46 53.91	24 07 57.0	76	10	0.001541	2.42	2.93	0.06	0.11	MHO 8
J034654.4+240642	3 46 54.40	24 06 42.6	11	4	0.000213	1.14	0.78	-0.16	0.23	U1125_01264261
J034655.0+240033	3 46 55.02	24 00 34.0	11	4	0.000210	0.83	0.74	0.11	0.19	...
J034655.3+240024	3 46 55.39	24 00 24.5	11	4	0.000210	0.73	0.68	0.11	0.17	...
J034655.4+241116	3 46 55.45	24 11 16.0	32	8	0.000646	1.43	1.90	-0.24	0.12	MHO 9
J034655.6+235622	3 46 55.70	23 56 22.8	20	6	0.001552	0.31	...	-0.23	0.16	HHJ 257
J034655.7+240151	3 46 55.76	24 01 51.5	28	6	0.000525	0.59	1.20	0.24	0.16	...
J034657.1+240337	3 46 57.10	24 03 37.5	11	4	0.000204	1.02	0.82	0.21	0.27	...

Table 1—Continued

CXOP	R.A. (J2000)	Decl. (J2000)	counts	error	count rate (cts s ⁻¹)	KS _s	KS _l	HR	σ_{HR}	Name ^a
J034657.3+240612	3 46 57.35	24 06 12.9	7	3	0.000132	0.52	0.42	0.31	0.28	...
J034658.1+240140	3 46 58.19	24 01 41.0	60	9	0.001134	1.04	0.84	-0.37	0.11	0346582+240141
J034659.2+240142	3 46 59.25	24 01 42.5	163	14	0.003087	1.91	1.63	-0.10	0.07	HHJ 299
J034659.9+240132	3 46 59.92	24 01 32.1	11	4	0.000209	1.02	0.61	-0.03	0.18	...
J034700.7+241322	3 47 00.76	24 13 22.3	46	9	0.000964	1.45	1.29	0.08	0.08	...
J034701.2+240206	3 47 01.30	24 02 06.0	41	7	0.000808	1.42	1.59	0.17	0.13	...
J034701.5+241047	3 47 01.58	24 10 47.5	46	8	0.000932	0.90	0.66	0.25	0.10	...
J034703.5+240934	3 47 03.54	24 09 34.7	433	24	0.008656	1.84	1.65	-0.28	0.04	HII 1280
J034704.0+235942	3 47 04.06	23 59 42.5	13	5	0.000269	0.53	0.37	-0.20	0.16	HII 1284
J034704.7+235748	3 47 04.80	23 57 48.3	20	6	0.000401	0.78	1.07	0.19	0.12	...
J034705.4+240608	3 47 05.42	24 06 08.7	12	4	0.000281	0.57	0.89	0.11	0.19	...
J034705.9+235943	3 47 05.91	23 59 43.5	47	8	0.000924	0.78	1.60	0.21	0.11	...
J034707.5+241013	3 47 07.54	24 10 13.7	54	9	0.001101	1.15	0.93	0.33	0.06	KECK
J034709.1+240307	3 47 09.12	24 03 07.6	376	21	0.007586	3.50	4.05	-0.19	0.05	SRS 60765
J034709.6+240146	3 47 09.69	24 01 46.6	25	6	0.000502	1.43	0.97	0.00	0.14	0347099+240149
J034710.1+240623	3 47 10.17	24 06 23.5	16	5	0.000398	0.53	0.41	0.00	0.17	...
J034711.2+240647	3 47 11.23	24 06 47.7	14	5	0.000278	0.83	1.19	0.26	0.14	...
J034711.7+240652	3 47 11.76	24 06 52.9	18	5	0.000359	0.69	0.74	0.23	0.15	...
J034711.8+241353	3 47 11.89	24 13 53.6	41	11	0.000885	0.93	0.63	-0.11	0.09	HHJ 92
J034712.5+240112	3 47 12.53	24 01 12.3	11	4	0.000223	0.93	0.87	0.09	0.17	...
J034712.7+240812	3 47 12.74	24 08 12.2	19	6	0.000410	1.48	1.20	-0.02	0.11	...
J034713.1+240045	3 47 13.17	24 00 45.2	13	5	0.000265	0.74	1.12	-0.24	0.11	0347131+240045
J034716.5+240741	3 47 16.53	24 07 41.9	277	19	0.005657	1.27	1.63	-0.40	0.05	HII 1338
J034716.9+241233	3 47 16.90	24 12 33.5	68	11	0.003017	0.72	...	0.12	0.10	...
J034718.0+240211	3 47 18.10	24 02 11.0	1158	37	0.023297	2.75	4.70	-0.15	0.03	HII 1355
J034722.6+240010	3 47 22.65	24 00 10.2	28	7	0.000579	1.02	0.75	0.10	0.08	...
J034725.3+240255	3 47 25.31	24 02 55.8	118	14	0.002442	1.16	0.73	-0.21	0.06	HHJ 427

^aOptical/IR name associated with each X-ray source. A blank entry denotes an AGN candidate.

Table 2. Position uncertainties.

Catalog	uncertainty ($''$)
Hertzsprung (1947) ^a	0.5
Haro et al. (1982)	30.0
Hambley et al. (1993)	10.0
Stauffer et al. (1994)	30.0
Micela et al. (1996)	30.0
Stauffer et al. (1998)	1.5
Micela et al. (1999)	15.0
Pinfield et al. (2000)	1.5
Martín et al. (2000)	1.0
Martín et al. (2001)	1.0
2MASS (2001)	1.0
USNO-A (2001)	0.5

^aAccurate positions for this catalog were derived by Eichhorn et al. (1970).

Table 3. Names for the previously catalogued *Chandra* detections.

CXOP	HII/ HHJ	SCG94/ MSK	MHO	BPL	KECK	2MASS	USNO-A	Other	Δ^a ($''$)
J034604.5+240957	BPL 88
J034612.5+240347	...	120 / 84
J034612.7+240314	HII 930	120 / 84	U1125_01258659	SRS 66387	3.57
J034615.8+241122	HII 956	122 / 86	U1125_01259068	HD 23479	2.38
J034619.4+235628 / 88
J034619.5+235653	HII 980	123 / 88	0346195+235653	U1125_01259575	Merope/HD 23480/23 Tau	0.93
J034620.1+240028	HII 989
J034620.8+235858	...	125 /
J034623.3+240151	HHJ 195	128 /	0346234+240151	1.17
J034623.6+235538	...	129 /	0346237+235540	2.51
J034625.2+240936	HHJ 429	130 / 90	0346253+240936	U1125_01260355	HCG 224/SRS 64388	1.05
J034627.9+235532	0346279+235525	6.44
J034628.8+235820	0346290+235822	2.42
J034629.1+240839	0346290+240839	2.49
J034630.1+240507	...	135 /	0346302+240507	...	SRS 64413	1.07
J034631.1+240701	HII 1061	136 / 94	0346311+240702	U1125_01261151	HCG 224/SRS 64400	1.07
J034632.0+235858	HII 1069	137 /	0346321+235858	...	HCG 225	1.21
J034632.4+240547	...	138 /
J034635.4+240134	HHJ 140	0346355+240135	1.32
J034635.8+235800	HII 1094	141 / 97	0346358+235801	...	HCG 227/SRS 64468	1.38
J034638.7+235804	0346388+235805	U1125_01262204	...	1.04
J034639.2+240610	HII 1122	144 / 103	0346393+240611	U1125_01262280	HD 23511/SRS 64407	1.00
J034639.3+240146	HII 1124	146 / 104	0346393+240146	U1125_01262279	...	1.02
J034640.6+240152	...	146 / 104	SRS 64425	...
J034641.3+240426	...	148 /
J034643.5+235941	...	149 / 107	0346435+235942	U1125_01262827	SRS 62618	1.29
J034643.6+240120	U1125_01262845	...	0.82
J034644.0+235911 / 107
J034646.6+240757	Yes	1.38
J034647.2+240128	...	151 /	Yes	1.67
J034647.9+240601	...	150 /
J034649.1+240833	Yes	1.47
J034651.3+240615	Yes	1.54
J034652.0+240005	Yes	1.55
J034653.0+235656	...	155 /	Yes	2.43
J034653.9+240757	MHO 8	...	Yes	0346539+240757	0.98

Table 3—Continued

CXOP	HII/ HHJ	SCG94/ MSK	MHO	BPL	KECK	2MASS	USNO-A	Other	Δ^a ($''$)
J034654.4+240642	U1125_01264261	...	2.15
J034655.4+241116	MHO 9	BPL 116	...	0346553+241116	1.93
J034655.6+235622	HHJ 257	155 /
J034658.1+240140	...	157 /	0346582+240141	1.01
J034659.2+240142	HHJ 299	157 /	0346593+240142	U1125_01264960	...	0.92
J034659.9+240132	...	157 /
J034703.5+240934	HII 1280	160 / 117	Yes	0347035+240935	U1125_01265582	HCG 249/SRS 62537	1.55
J034704.0+235942	HII 1284	... / 118	0347042+235942	U1125_01265693	HD 23585/SRS 62623	2.08
J034705.9+235943 / 118
J034707.5+241013	...	163 /	Yes	4.75
J034709.1+240307	...	166 /	0347091+240307	...	SRS 60765	0.65
J034709.6+240146	0347099+240149	4.29
J034711.8+241353	HHJ 92	...	HHJ 92	BPL 131	...	0347118+241354	0.65
J034713.1+240045	0347131+240045	U1125_01266937	...	0.24
J034716.5+240741	HII 1338	170 / 128	0347165+240742	...	HD 23608	0.39
J034716.9+241233	...	171 /
J034718.0+240211	HII 1355	172 / 130	0347181+240211	...	HCG 262/SRS 60774	0.58
J034725.3+240255	HHJ 427	179 /	0347253+240257	1.25

| 32 |

Note. — HII: Hertzsprung (1947) catalog. HHJ: Hambly et al. (1993) catalog. SCG94: *ROSAT* catalog in Stauffer et al. (1994). MSK: *ROSAT* catalog in Micela et al. (1996). MHO: Mount Hopkins Observatory sources in Stauffer et al. (1998). BPL: Burrell Pleiades candidates as designated by Pinfield et al. (2000). KECK: Sources detected by Eduardo Martín with the Keck II Telescope (Martín et al. 2001, see Paper I). 2MASS: Second Incremental Release of the Point Source Catalog (2MASS 2001). USNO-A: Catalog A from the US Naval Observatories (USNO-A 2001). Other: Additional references given by the SIMBAD database.

^aOffset from optical or IR counterparts from Keck astrometry (Krishnamurthi et al. 2001), 2MASS (2MASS 2001), or USNO (USNO-A 2001), in order of preference.

Table 4. IR and optical data for *Chandra* sources.

CXOP	Name	$\log L_X$ (erg s $^{-1}$)	B	V	R	I	J	H	K	MK	Status ^a
J034604.5+240957	BPL 88	15.74	NM
J034612.7+240314	HII 930	29.08	15.30	14.08	14.20	12.60	K V	PM
J034615.8+241122	HII 956	29.31	8.12	7.84	8.30	A7 V	PM
J034619.5+235653	HII 980	29.6	3.96	4.06	4.20	B6 IVn	PM
J034623.3+240151	HHJ 195	28.13	...	18.5	17.50	15.10	13.71	13.07	12.77	...	PC
J034623.6+235538	0346237+235540	16.98	16.10	15.22	...	AGN
J034625.2+240936	HHJ 429	29.19	18.00	16.00	14.70	13.20	12.01	11.36	11.11	M	PM
J034627.9+235532	0346279+235525	14.79	14.30	14.03	...	AGN
J034628.8+235820	0346290+235822	13.06	12.65	12.48	...	NM
J034629.1+240839	0346290+240839	16.00	15.13	14.85	...	AGN
J034630.1+240507	SRS 64413	...	17.06	16.07	12.87	12.28	12.06	...	NM
J034631.1+240701	HII 1061	29.06	14.64	13.49	13.30	12.26	11.27	10.60	10.44	K5 V	PM
J034632.0+235858	HII 1069	...	14.30	14.55	10.55	9.88	9.69	K3 V	NM
J034635.4+240134	HHJ 140	29.48	...	19.00	17.80	15.40	13.68	13.11	12.83	M V	PC
J034635.8+235800	HII 1094	29.19	15.26	13.90	...	12.34	11.50	10.84	10.66	K V	PM
J034638.7+235804	0346388+235805	...	17.30	...	15.80	...	14.25	13.69	13.50	...	NM
J034639.2+240610	HII 1122	29.06	9.59	9.17	9.70	...	8.43	8.22	8.18	F4 V	PM
J034639.3+240146	HII 1124	29.27	13.14	12.20	12.50	11.39	10.45	9.97	9.85	K3 V	PM
J034640.6+240152	SRS 64425	27.85	13.21	12.27	K2 V	PM
J034643.5+235941	SRS 62618	28.67	17.63	16.12	15.10	...	12.45	11.85	11.54	...	PC
J034643.6+240120	U1125_01262845	...	19.70	...	17.30	NM
J034646.6+240757	KECK	22.39	22.19	AGN
J034647.2+240128	KECK	21.64	21.21	AGN
J034649.1+240833	KECK	22.07	21.72	AGN
J034652.0+240005	KECK	20.66	20.67	AGN
J034653.0+235656	KECK	20.29	19.84	AGN
J034653.9+240757	MHO 8	28.52	...	18.92	...	15.76	14.10	13.48	13.20	M V	PM
J034654.4+240642	U1125_01264261	...	17.40	...	14.30	NM
J034655.4+241116	MHO 9	27.92	...	19.02	...	15.55	13.78	13.22	12.89	M V	PM
J034655.6+235622	HHJ 257	28.32	...	18.40	17.00	14.70	PC
J034658.1+240140	0346582+240141	13.95	13.27	12.95	M V	NM
J034659.2+240142	HHJ 299	28.72	19.90	17.60	16.60	14.40	13.00	12.38	12.12	M V	PM
J034703.5+240934	HII 1280	29.01	15.85	14.45	13.80	12.84	11.63	10.96	10.76	K7.5	PM
J034704.0+235942	HII 1284	27.58	8.51	8.25	8.70	...	7.76	7.68	7.63	A9 V	PM
J034707.5+241013	KECK	23.80	23.49	AGN
J034709.1+240307	SRS 60765	29.03	18.33	16.52	12.59	11.94	11.73	...	PC
J034709.6+240146	0347099+240149	16.39	15.63	15.16	...	AGN
J034711.8+241353	HHJ 92	28.17	...	19.52	18.60	15.87	14.03	13.51	13.20	...	PM
J034713.1+240045	0347131+240045	...	18.60	...	19.10	...	14.88	14.18	13.91	...	NM
J034716.5+240741	HII 1338	28.67	8.99	8.57	7.74	7.58	7.50	F3 V	PM
J034718.0+240211	HII 1355	29.56	15.26	13.90	...	12.25	11.05	10.36	10.19	K6n	PM
J034725.3+240255	HHJ 427	28.53	...	17.60	15.20	14.60	12.65	12.03	11.79	M V	PM

^aPleiades members (PM) and Pleiades candidates are determined using the proper motion probability and photometric properties as listed by Stauffer et al. (1998), Belikov et al. (1998), Micela et al. (1996), Schilbach et al. (1995), and Hambly et al. (1993) (§3.1.1). Non-members (NM) are sources where $\log(f_x/f_v) \leq -1.0$ that do not show any of the characteristics of a Pleiades star. AGN candidates (AGN) have $-1.0 \leq \log(f_x/f_v) \leq 1.2$.

Table 5. Pleiades members not detected by *Chandra*.

Name	$\log L_X$ (erg s $^{-1}$)	B	V	R	I	J	H	K	MK
MHO 10	< 27.84	...	20.18	...	16.87	15.00	14.41	14.06	...
MHO 11	< 28.17	...	21.44	...	16.98	14.84	14.20	13.99	...
HCG 254	< 28.17	...	19.34	18.60	16.00	14.26	13.72	13.45	K0 V
HII 1362	< 27.87	8.50	8.25	7.73	7.68	7.63	A7
HII 1375	< 27.98	6.30	6.29	6.21	6.28	6.27	A0 V

Table 6. Spectral information for six X-ray bright Pleiades members.

Name	MK	kT ₁ (keV)	EM ₁ (10^{52}cm^{-3})	kT ₂ (keV)	EM ₂ (10^{52}cm^{-3})	Ne	Mg	Si	Fe	χ^2	Date
HII 1094	K V	0.48 ± 0.04	0.7 ± 0.2	1.00	1.00	1.00	0.25 ± 0.08	0.90	1999 Sep 18
HII 1094	K V	0.62 ± 0.06	0.7 ± 0.1	3.5	0.4	2.50 ± 0.45	1.00	2.00 ± 0.50	0.52 ± 0.14	0.75	2000 Mar 20
HII 1124	K3 V	0.34 ± 0.02	1.1 ± 0.2	3.5	0.4	1.00	1.00	1.00	0.23 ± 0.07	0.84	1999 Sep 18
HII 1124	K3 V	0.66 ± 0.05	1.3 ± 0.3	1.00	1.00	1.00	0.19 ± 0.06	0.77	2000 Mar 20
HII 1355	K6	0.33 ± 0.02	0.9 ± 0.1	3.5	1.3	2.59 ± 0.32	1.00	3.00 ± 1.00	0.55 ± 0.15	0.83	1999 Sep 18
HII 1355	K6	0.40 ± 0.05	1.0 ± 0.6	3.5	0.8	1.83 ± 0.61	1.00	1.00	0.16 ± 0.12	0.84	2000 Mar 20
HII 1122	F4 V	0.45 ± 0.04	0.6 ± 0.1	1.00	2.79 ± 0.74	1.00	1.00	1.09	2000 Mar 20
HII 956	A7 V	0.57 ± 0.01	1.4 ± 0.1	1.50 ± 0.30	1.50 ± 0.30	1.00	1.00	1.61	1999 Sep 18
HII 980	B6 IV	0.53 ± 0.02	2.4 ± 0.2	1.50 ± 0.30	1.50 ± 0.20	1.50 ± 0.20	0.63 ± 0.05	0.93	1999 Sep 18
HII 980	B6 IV	0.59 ± 0.02	1.6 ± 0.6	1.00	1.39 ± 0.50	1.69 ± 0.74	0.69 ± 0.17	1.05	2000 Mar 20

Table 7. X-ray properties of Pleiades members in the *Chandra* FOV.

Name	CXOP	MK	V	B–V	V–I	$\log L_X$ (ergs s^{-1})	HR	KS _s	Variability
Inactive star sample									
HII 1375	...	A0 V	6.29	0.01	...	<27.98
HII 1284	J034704.0+235942	A9 V	8.25	0.26	...	27.58	-0.20	0.53	No
HII 1362	...	A7	8.25	0.25	...	<27.87
SRS 64425	J034640.6+240152	K2 V	12.27	0.94	...	27.85	0.22	0.65	No
HCG 254	19.34	...	3.34	<28.17
HHJ 92	J034711.8+241353	...	19.52	...	3.65	28.17	-0.11	0.93	No
MHO 10	...	M	20.18	...	3.31	<27.84
MHO 11	...	M	21.44	...	4.46	<28.17
Active K star sample									
HII 1124	J034639.3+240146	K3 V	12.20	0.94	0.81	29.27	-0.22	1.32	Yes
HII 1061	J034631.1+240701	K5 V	13.49	1.15	1.23	29.06	-0.21	1.70	flaring
HII 1355	J034718.0+240211	K6	13.90	1.36	1.65	29.56	-0.15	2.75	flaring
HII 1094	J034635.8+235800	K V	13.90	1.36	1.56	29.19	-0.25	3.24	flaring
HII 930	J034612.7+240314	K V	14.08	1.22	1.48	29.08	-0.19	1.59	flaring
HII 1280	J034703.5+240934	K7.5	14.45	1.40	1.61	29.01	-0.28	1.84	flaring
Active B6-F4 star sample									
HII 980	J034619.5+235653	B6 IVn	4.06	-0.10	...	29.60	-0.34	1.91	Yes
HII 956	J034615.8+241122	A7 V	7.84	0.28	...	29.31	-0.48	1.91	Yes
HII 1338	J034716.5+240741	F3 V	8.57	0.42	...	28.67	-0.40	1.27	Yes
HII 1122	J034639.2+240610	F4 V	9.17	0.42	...	29.06	-0.49	1.55	Yes
Active M star sample									
HHJ 429	J034625.2+240936	M	16.00	2.00	2.80	29.19	-0.11	2.53	flaring
HHJ 299	J034659.2+240142	M V	17.60	2.30	3.20	28.72	-0.10	1.91	flaring
HHJ 427	J034725.3+240255	M V	17.60	...	3.00	28.53	-0.21	1.16	flaring
MHO 8	J034653.9+240757	M V	18.92	...	3.16	28.52	0.06	2.42	flaring
MHO 9	J034655.4+241116	M V	19.02	...	3.47	27.92	-0.24	1.43	Yes
Possible Members ^a									
SRS 62618	J034643.5+235941	...	16.12	1.51	...	28.67	-0.23	1.33	flaring
SRS 60765	J034709.1+240307	...	16.52	1.81	...	29.03	-0.19	3.50	flaring
HHJ 257	J034655.6+235622	...	18.40	...	3.70	28.32	-0.23	0.31	No
HHJ 195	J034623.3+240151	...	18.50	...	3.40	28.13	-0.24	1.52	Yes
HHJ 140	J034635.4+240134	M V	19.00	...	3.60	29.48	0.17	13.65	flaring

^aX-ray luminosities are computed assuming that the stars are located at the distance of the Pleiades (127 pc).